Inelastic deformation micromechanism and modified fragmentation model for silicon carbide under dynamic compression

Zhiyong Wang [a], Peifeng Li [b,*], Weidong Song [c]

[a] School of Mechatronical Engineering, Beijing Institute of Technology, Beijing, China

[b] School of Engineering, University of Glasgow, Glasgow, UK

[a] State Key Laboratory of Explosion Science and Technology, Beijing Institute of Technology, Beijing, China

[*] Corresponding author's email: peifeng.li@glasgow.ac.uk (P. Li); Tel: +44 141 330 2703.

Abstract

The underlying micromechanism remains to be clarified for the bulk inelastic behaviour of specific ceramics under impact loads. In this study, the silicon carbide materials were subjected to the split-Hopkinson pressure bar compression in which the strain rate was not constant but increased to the dynamic level at high stresses. The inelastic deformation occurs in the high strain rate stage in compression, followed by the final transgranular fracture. The post-test fragments were examined in both the SEM and high resolution TEM. It was found that macroscopic inelastic behaviour is dominated by the dislocation motion and the localised amorphisation that arise at high strain rates. The damage and thus the degraded modulus in the dynamic inelastic deformation were incorporated to modify a dynamic fragmentation model to evaluate the fragment size as a function of strain rates. The modified model more accurately predicts the size of fragments produced at high strain rates.

Keywords: Silicon carbide; Inelastic deformation; Fragmentation; Dislocations; Amorphisation.

1 Introduction

Silicon carbide ceramics possess the excellent properties for high speed applications, such as high strength-to-weight ratio, high hardness, low compressibility and superior ballistic performance [1-5]. They have been utilised in the layered armour systems to dissipate impact energy [1, 2]. Evaluation of the energy dissipation capacity requires a better understanding of the underlying micromechanism of deformation and failure in the ceramic subjected to dynamic impact loads.

Plentiful experimental and numerical studies have been reported on the dynamic deformation and failure mechanisms in various length scales in different ceramics [6-15]. The split-Hopkinson pressure bar (SHPB) experiments and subsequent analysis of measured strain waves have been investigated to accurately determine bulk dynamic stress–strain responses of ceramic materials [6, 16]. A large portion of research focused on the phenomena in the microscopic scale such as micro-crack initiation and propagation that account for macro-cracking and fragmentation in the final fracture [3, 7, 10, 17-20]. The micro-crack propagation is significantly affected by the heterogeneities such as inclusions. The localised tensile stress concentrated near grain boundaries and inclusions drive micro-cracks to nucleate and grow to a subcritical state; the macroscopic failure finally occurs as a result of the coalescence of micro-cracks [10, 21]. The loading rate plays a crucial role in the failure process for a specific ceramic material [1, 9, 10, 22-24]. The fracture mode in ceramics can be intergranular, transgranular or a combination of both, depending on intrinsic heterogeneities and extrinsic loading rates [8, 10, 20, 22, 25-27]. The size of

fragments collected in dynamic impact tests often follows a statistic distribution, and is strongly affected by the strain rate; the fragment size reduces with the increasing strain rate [7, 10]. Various analytical models have been proposed for the dynamic fragmentation in ceramics [7, 9, 23, 28]. However, some of the constitutive parameters (e.g., Young's modulus) have usually been assumed constant in these analytical models, thus leading to the inaccuracy of predictions. In fact, the material properties can vary as a function of loading conditions during the dynamic impact process, e.g., the degradation of the bulk Young's modulus at high rates in ceramics. A more reliable dynamic fragmentation model need to incorporate the evolution of these properties.

Bulk inelastic behaviour and microscopic localised softening have been observed in various ceramic materials under shock wave loading [8-10, 16, 17, 25, 29]. The dislocation motion at room temperature gives rise to significant plastic deformation prior to the final fracture [3, 27, 30]. Dislocation activities near grain boundaries dominate the dynamic deformation mechanism in polycrystalline ceramics, often resulting in the intergranular fracture mode. At the very high loading rate, deformation twinning can become a prevalent mechanism, and the twinning interface serves as the preferred cleavage plane for the transgranular fracture [17, 25]. Numerical models at the atomic level such as molecular dynamics have been developed to explore the physical mechanism for inelastic behaviour [31]. However, only a very small domain can be simulated in the model, thus limiting the exploration of the inelastic phenomena. Therefore, the debate still continues on the underlying

micromechanisms of the dynamic inelastic behaviour, even for ceramic materials of the same chemical compositions but fabricated by the different processes.

The aim of the study reported here is to investigate the physical phenomena in the microscopic scale for the inelastic behaviour of silicon carbide, and then develop a dynamic fragmentation model. The SHPB experiments were performed on silicon carbide specimens to quantitatively characterise the bulk deformation process and identify the inelastic deformation stage. The fragments collected in the SHPB tests were examined in the scanning electron microscope (SEM) to analyse the size distribution statistically. The thin fracture edge in the fragments was further examined in high resolution transmission electron microscope (TEM) to explore the change in crystalline structures during dynamic deformation.

2 Experimental procedure

The dynamic uniaxial compression experiments of hot-pressed cylindrical silicon carbide specimens of the diameter 5 mm and the length 5 mm (Chair Man Hi-Tech Co. Ltd., Taiwan) were performed in an in-house split-Hopkinson pressure bar system using YAG300 maraging steel striker, input and output bars (diameter 20 mm). The silicon carbide material was >97% in purity with a density of 3100 kg m^{-3}. The SHPB system as well as the subsequent analysis of measured strain waves was developed for the accurate measurement of dynamic behaviour of ceramics as detailed in the previous work [6]. A pair of wave impedance-matched cylindrical tungsten carbide inserts (diameter 17 mm) was laterally confined by the

steel sleeves and sandwiched between the bars and the specimen to prevent the indentation into the steel bars by the harder silicon carbide specimen. To achieve the highest possible strain rate at a level of $>10^3$ s^{-1}, no pulse shaping technique was applied in the SHPB tests. For comparison, the quasi-static uniaxial compression tests of specimens (diameter 5 mm and length 12 mm) were conducted in an INSTRON 5569 (INSTRON, MA, USA) electromechanical universal testing machine. The details on both the SHPB and INSTRON tests of high strength ceramics can be found in the previous work [6, 10].

Prior to the compression experiments, the specimen surfaces were examined in the optical microscope to avoid the early failure due to surface defects; and only the specimens without surface defects were tested. The specimen ends were lubricated with Castrol LMX grease to minimise the interfacial friction. In the tests, an in-house acrylic transparent enclosure box was used to encompass and protect the specimen setup and to collect the fragments after failure. At least ten specimens were tested for the compression at the quasi-static and dynamic rates.

After the uniaxial compression experiments, the collected specimen fragments were examined in a JEOL JSM-5600LV SEM (JEOL Ltd., Japan) to reveal the fracture features. The small fragments obtained from the SHPB tests were found to have the very thin edges that are electron transparent and thus ideal for inspection in TEM [17, 25]. Some of these small fragments were dispersed in isopropanol alcohol via sonication for 5 minutes. The dispersion was deposited onto the carbon coated copper grid via drop casting, and followed by the evaporation of the isopropanol

alcohol. Note that the drop casting method was non-destructive to the fragments. The thin edges of the small fragments were characterised in a JEOL JEM-2100F high resolution TEM.

3 Results and discussion

3.1 Dynamic deformation and failure process

The measured strain waves in the SHPB tests were analysed to calculate the histories of stress and strain of the silicon carbide specimen as shown in Fig. 1(a) [6]. As the specimen is dynamically compressed in the SHPB, the instantaneous strain rate (the slope of the strain versus time curve) increases from zero to the dynamic level. The strain rate reaches around 500 s^{-1} at the stress ~2000 MPa, and continues increasing to approximately 2500 s^{-1} prior to the fracture (Fig. 1(a)). Fig. 1(b) compares the typical stress–strain response of silicon carbide at the quasi-static and dynamic loading rates. A good test repeatability was achieved for the silicon carbide specimens with the good surface quality. Under quasi-static compression, the strain rate of 10^{-5} s^{-1} is constant and only elastic deformation occurs before failure. In the SHPB compression, the initial linear elastic deformation is followed by the inelastic behaviour especially when the stress reaches ~2000 MPa and the strain rate is >500 s^{-1}. The dynamic (or high) strain rate in this study refers to the rate above 500 s^{-1}. Both the compressive strength and strain at fracture increase with the loading rates (Fig. 1(b)), indicating a higher energy dissipation capacity of silicon carbide under dynamic loads. The quasi-static compressive strength of approximately 2800 GPa is

consistent with the data of silicon carbide fabricated by the similar process reported in the literature [9].

Fig. 2 compares the fragments collected from the quasi-static and dynamic compression experiments. The fragments are much smaller in the SHPB. Similar phenomena were also observed in other polycrystalline ceramics, e.g., alumina [10]. As shown in Fig. 3, the fracture surfaces observed in the SEM are smooth in the fragments obtained in both the low and high rates; this suggest that the fracture in silicon carbide is predominantly transgranular in the two rates. However, it should be noted that dissimilar macroscopic deformation behaviour are observed in the quasi-static and dynamic compression. Prior to the final fracture (specimen collapse), the significantly inelastic behaviour occurs in the high loading rates (Fig. 1(b)). As a result, it is essential to reveal the underlying micromechanism of this inelastic behaviour in silicon carbide subjected to dynamic compression.

3.2 Inelastic deformation micromechanism: dislocation motion and localised amorphisation

The Hugoniot elastic limit (e.g., 8±3 GPa for silicon carbide [32]) is an important parameter to differentiate the transition from the elastic to plastic response prior to failure. However, the present research found that this transition arises in silicon carbide materials at the stress level (approximately 2000 MPa in Fig. 1(b)) that is much lower than the Hugoniot elastic limit. This phenomena may be attributed to several micromechanisms in ceramics, such as initiation and propagation of

micro-cracks, plastic deformation, and phase transformation [8, 17, 18, 25]. The wing crack mechanism has been typically used to understand the compressive failure process of brittle materials [9, 10]. Tensile tresses are localised near the grain boundaries or defects (e.g., voids) in silicon carbide. Micro-cracks nucleate at the tip of these tensile stress concentration areas and grow to increase the mode I stress intensity factor. The coalescence of these compression-induced, interacting tensile micro-cracks thus results in the macroscopic failure process (i.e., macro-cracking) of silicon carbide. The bright field TEM image in Fig. 4(a) illustrates a wing-like micro-crack in silicon carbide subjected to dynamic compression. It appears that this micro-crack initiates at the triple grain junctions, because there are no internal defects observed, e.g., voids or inclusions.

Meanwhile, the high density dislocations as shown in the bright and dark field TEM images imply the excessive local strain energy especially in the vicinity of the crack tip (Fig. 4(b)). The motion of these dislocations produces plastic deformation, as demonstrated by the bulk inelastic behaviour (Fig. 1(b)). With the strain energy accumulated to a considerably high level, the sudden release of the strain energy drives the micro-crack to propagate simultaneously, and thus leads to the final failure of silicon carbide (transgranular fracture and macroscopic fragmentation).

The periodic crystal lattice observed in the high resolution TEM indicates that silicon carbide undergoes extensive elastic deformation during dynamic compression (refer to Fig. 5). However, the loss of the crystalline structure (amorphisation) is also found in the regions as highlighted by the simple closed curves. Fast Fourier

transformation (FFT) performed on these highlighted regions results in a diffuse halo ring, confirming the amorphous (noncrystalline) phase in them (refer to inset i in Fig. 5), while the FFT on the lattice matrix shows the expected reciprocal lattice (inset ii in Fig. 5). The electron energy loss spectroscopy on the amorphous regions and the crystalline matrix reveals the same chemical composition in both of them, suggesting that no chemical reaction or decomposition occurs in the amorphous phases. Instead, the amorphous phase is the result of dynamic loading.

As the macroscopic inelastic behaviour is observed at the relatively high stress level (Fig. 1), it can be concluded that the dislocation motion and the amorphisation process occur at the high strain rate stage in the SHPB test (note that the strain rate increases to the high level in the test as in Fig. 1(a).). Molecular dynamic simulations suggest that the dislocation motion becomes jagged at high strain rates and then the phase transition occurs [33]. The high resolution TEM observations reported here provide the evidence that the high rate deformation in silicon carbide is inelastic due to the dislocation motion and the amorphisation under the impact condition.

3.3 Modified model of dynamic fragmentation

The silicon carbide fragments collected from each SHPB test were dispersed to avoid overlapping and re-examined in the SEM in order to characterise their geometries quantitatively. The typical fragments are of an approximately parallelepiped shape (Fig. 2(c)). The SEM images of the separate fragments were processed in the ImageJ software to quantify the projected area A of individual

fragments. The fragment width was determined by the average of the minimum (W_{min}) and maximum (W_{max}) widths (refer to Fig. 2(c)). Therefore, the size (i.e., length, L) of the individual fragment was estimated as follows.

$$L = \frac{A}{(W_{min} + W_{max})/2} \tag{1}$$

The statistical analysis was carried out on the size of individual fragments collected from each SHPB test.

Fig. 6 shows the calculated empirical probability density function (PDF) and cumulative distribution function (CDF) of the fragments in one of the SHPB tests. The Kolmogorov–Smirnov test was performed on the statistical analysis of fragment size; similar size distribution was found for the fragments from the individual SHPB tests. The log-normal distribution was used to fit the size distribution of fragments, with the probability density function $f(L)$ given as [34],

$$f(L) = \frac{1}{\sqrt{2\pi}\sigma L}\exp\left(\frac{-(\ln(L)-\mu)^2}{2\sigma^2}\right) \tag{2}$$

where μ and σ are the mean and standard deviation of the natural logarithm ln(L), respectively. The probability density is presented at the 95% confidence level in Fig. 6. For the majority of the fragments, their size ranges from 100 μm to 400 μm. The probability for the large (L > 400 μm)and small (L < 100 μm) fragments is extremely low probably because of the short durations at the low and high stress (and thus strain rate) levels in the SHPB test (Fig. 1(a)). The previous finite element simulation of the ceramic subjected to SHPB compression revealed that the instantaneous release of the compressive strain energy stored in the specimen centre is

significantly high to comminute the ceramic material into small fragments [10]. This could be responsible to the low probability of the large fragments. The highest strain rate level that can be achieved prior to the specimen failure determines the low probability for the small fragments.

The dynamic fragmentation model has been proposed to predict the size of ceramic fragments arising at the applied strain rate $\dot{\varepsilon}$, using the material properties through the intermediate variables α, θ and β [9, 23, 28],

$$L = 4\sqrt{\frac{\alpha}{3}}\sinh\left(\frac{\theta}{3}\right) \tag{3}$$

in which

$$\alpha = \frac{3\sigma_{\max}^2}{E\rho\dot{\varepsilon}^2} \tag{4}$$

$$\theta = \sinh^{-1}\left(\beta\left(\frac{3}{\alpha}\right)^{3/2}\right) \tag{5}$$

and

$$\beta = \frac{3}{2}\left(\frac{K_{\mathrm{IC}}}{\rho c_{\mathrm{d}}\dot{\varepsilon}}\right)^2 \tag{6}$$

where $\sigma_{\max}$ is the tensile strength, E is the Young's modulus, ρ is the density, K_{IC} is the fracture toughness, and c_{d} is the longitudinal wave velocity. During the dynamic inelastic process in the SHPB test, the Young's modulus is not constant, but degrades with the increasing stress and strain rate (Fig. 1(a)) owing to the amorphisation, dislocation motion and micro-crack propagation in the silicon carbide. The use of constant Young's modulus thus overestimates the fragment size, especially at the high

strain rate stage. To correct this overestimation, the modulus E_D was proposed to degrade as a linear function of the damage D in the present study,

$$E_D = E(1-D) \tag{7}$$

while the damage evolves with the strain rate in an exponential form,

$$D = 1 - \exp\left(-k\frac{\dot{\varepsilon}}{\dot{\varepsilon}_0}\right) \tag{8}$$

where k is the damage evolution parameter and $\dot{\varepsilon}_0$ is the reference strain rate. Thus Eq. 4 can be rewritten to incorporate the effect of damage evolution in dynamic compression.

$$\alpha = \frac{3\sigma_{\max}^2}{E_D \rho \dot{\varepsilon}^2} \tag{9}$$

The dynamic fragmentation model expressed by Eq. 3 can be modified using the degraded modulus (Eq. 9) instead of the constant modulus (Eq. 4).

Fig. 7 demonstrates the fragment size predicted by the damage-incorporated dynamic fragmentation model using the properties of silicon carbide as listed in Table 1. Note that this model was developed for dynamic strain rates and may not be applicable to quasi-static rates; the prediction at the low rates in Fig. 7 is only illustrative. If the damage evolution in the dynamic compression is taken into account in the model, the predicted fragment size falls in the range of approximately 100–400 μm, which is consistent with dynamic fragmentation observed in the SHPB tests (strain rate up to 2500 s^{-1}). If the damage is excluded but a constant Young's modulus is used, the constant fragment size (approximately 400 μm) is predicted for

the strain rate <2500 s^{-1}, an overestimation to the actual observations. Therefore, the incorporation of damage evolution into the modified fragmentation model enables the accurate prediction of the size of fragments produced in the dynamic compression such as SHPB tests.

4 Conclusions

The micromechanism of dynamic inelastic behaviour in silicon carbide was investigated in the SHPB experiments and electron microscopes on post-test fragments. The dynamic fragmentation was statistically analysed and then modelled as a function of strain rate. The following conclusions are drawn.

- The strain rate is not constant during the SHPB compression, but reaches the dynamic level at the high stress state and continues increasing prior to the final fracture. The dynamic inelastic behaviour occurs at the high strain rate stage. It was found that the dislocation motion and localised amorphisation (the loss of crystalline structure) are the micromechanisms that determine the bulk dynamic inelastic behaviour in silicon carbide.

- The final fracture mode is predominantly transgranular. The size of fragments collected in the SHPB tests follows the log-normal distribution.

- The material properties such as the modulus can degrade with the damage at the high strain rate in the dynamic inelastic deformation. The modified dynamic fragmentation model incorporating damage evolution predicts the

fragment size at high strain rates more accurately, compared to the model without considering the damage.

Acknowledgements

The authors gratefully acknowledge the financial support of Academic Research Fund (AcRF) Tier 1 by Ministry of Education in Singapore, the National Key Research and Development Programme of China (2016YFC0801200) and the National Natural Science Foundation of China (11672043 and 11521062). ZW thanks the Research Student Scholarship by Nanyang Technological University in Singapore where this work was conducted.

Data availability

The raw/processed data required to reproduce these findings cannot be shared at this time as the data also forms part of an ongoing study.

References

[1] W.W. Chen, A.M. Rajendran, B. Song, X. Nie, Dynamic fracture of ceramics in armor applications, J. Am. Ceram. Soc. 90(4) (2007) 1005-1018.

[2] A.J. Harris, B. Vaughan, J.A. Yeomans, P.A. Smith, S.T. Burnage, Surface preparation of silicon carbide for improved adhesive bond strength in armour applications, J. Eur. Ceram. Soc. 33(15-16) (2013) 2925-2934.

[3] C.J. Shih, M.A. Meyers, V.F. Nesterenko, S.J. Chen, Damage evolution in dynamic deformation of silicon carbide, Acta Mater. 48(9) (2000) 2399-2420.

[4] J.L. Zinszner, P. Forquin, G. Rossiquet, Experimental and numerical analysis of the dynamic fragmentation in a SiC ceramic under impact, Int. J. Impact Eng. 76 (2015) 9-19.

[5] Y. Zhang, L.T. Zhang, X.W. Yin, Y.S. Liu, Z.B. He, J.X. Zhang, Effects of porosity on in-plane and interlaminar shear strengths of two-dimensional carbon fiber reinforced silicon carbide composites, Mater. Des. 98 (2016) 120-127.

[6] Z. Wang, P. Li, Characterisation of dynamic behaviour of alumina ceramics: evaluation of stress uniformity, AIP Adv. 5(10) (2015) 16.

[7] S. Maiti, K. Rangaswamy, P.H. Geubelle, Mesoscale analysis of dynamic fragmentation of ceramics under tension, Acta Mater. 53(3) (2005) 823-834.

[8] K.M. Reddy, P. Liu, A. Hirata, T. Fujita, M.W. Chen, Atomic structure of amorphous shear bands in boron carbide, Nat. Commun. 4 (2013) 5.

[9] H. Wang, K.T. Ramesh, Dynamic strength and fragmentation of hot-pressed silicon carbide under uniaxial compression, Acta Mater. 52(2) (2004) 355-367.

[10] Z. Wang, P. Li, Dynamic failure and fracture mechanism in alumina ceramics: Experimental observations and finite element modelling, Ceram. Int. 41(10) (2015) 12763-12772.

[11] K.S. Zhang, D. Zhang, R. Feng, M.S. Wu, Microdamage in polycrystalline ceramics under dynamic compression and tension, J. Appl. Phys. 98(2) (2005) 10.

[12] S. Acharya, S. Bysakh, V. Parameswaran, A.K. Mukhopadhyay, Deformation and failure of alumina under high strain rate compressive loading, Ceram. Int. 41(5) (2015) 6793-6801.

[13] P. Badica, D. Batalu, M. Burdusel, M.A. Grigoroscuta, G.V. Aldica, M. Enculescu, R.A. Gabor, Z.Y. Wang, R.X. Huang, P.F. Li, Compressive properties of pristine and SiC-Te-added MgB2 powders, green compacts and spark-plasma-sintered bulks, Ceram. Int. 44(9) (2018) 10181-10191.

[14] L.B. Brown, P.J. Hazell, I.G. Crouch, J.P. Escobedo, A.D. Brown, Computational and Split-Hopkinson Pressure -Bar studies on the effect of the jacket during penetration of an AK47 bullet into ceramic armour, Mater. Des. 119 (2017) 47-53.

[15] P. Shukla, S. Robertson, H. Wu, A. Telang, M. Kattoura, S. Nath, S.R. Mannava, V.K. Vasudevan, J. Lawrence, Surface engineering alumina armour ceramics with laser shock peening, Mater. Des. 134 (2017) 523-538.

[16] H. Zhao, G. Gary, On the use of SHPB techniques to determine the dynamic behavior of materials in the range of small strains, Int. J. Solids Struct. 33(23) (1996) 3363-3375.

[17] M.W. Chen, J.W. McCauley, D.P. Dandekar, N.K. Bourne, Dynamic plasticity and failure of high-purity alumina under shock loading, Nat. Mater. 5(8) (2006) 614-618.

[18] K.M. Reddy, J.J. Guo, Y. Shinoda, T. Fujita, A. Hirata, J.P. Singh, J.W. McCauley, M.W. Chen, Enhanced mechanical properties of nanocrystalline boron carbide by nanoporosity and interface phases, Nat. Commun. 3 (2012) 7.

[19] Y.C. Wu, N.J. Ho, H.Y. Lu, Dissociation of basal dislocations in hexagonal barium titanate, J. Microsc. 220 (2005) 205-220.

[20] J. Pittari, G. Subhash, J. Zheng, V. Halls, P. Jannotti, The rate-dependent fracture toughness of silicon carbide- and boron carbide-based ceramics, J. Eur. Ceram. Soc. 35(16) (2015) 4411-4422.

[21] Z. Wang, P. Li, Voronoi cell finite element modelling of the intergranular fracture mechanism in polycrystalline alumina, Ceram. Int. 43(9) (2017) 6967-6975.

[22] A. Belenky, I. Bar-On, D. Rittel, Static and dynamic fracture of transparent nanograined alumina, J. Mech. Phys. Solids 58(4) (2010) 484-501.

[23] W.J. Drugan, Dynamic fragmentation of brittle materials: analytical mechanics-based models, J. Mech. Phys. Solids 49(6) (2001) 1181-1208.

[24] P. Badica, S. Grasso, H. Borodianska, S.S. Xie, P.F. Li, P. Tatarko, M.J. Reece, Y. Sakka, O. Vasylkiv, Tough and dense boron carbide obtained by high-pressure (300 MPa) and low-temperature (1600 degrees C) spark plasma sintering, J. Ceram. Soc. Jpn. 122(1424) (2014) 271-275.

[25] M.W. Chen, J.W. McCauley, K.J. Hemker, Shock-induced localized amorphization in boron carbide, Science 299(5612) (2003) 1563-1566.

[26] J.C. LaSalvia, J.W. McCauley, Inelastic deformation mechanisms and damage in structural ceramics subjected to high-velocity impact, Int. J. Appl. Ceram. Technol. 7(5) (2010) 595-605.

[27] Z.L. Tian, L.Y. Zheng, J.M. Wang, J.B. Yang, G. Yang, J.Y. Wang, Damage tolerance and extensive plastic deformation of -Yb2Si2O7 from room to high temperatures, J. Am. Ceram. Soc. 98(9) (2015) 2843-2851.

[28] L.A. Glenn, A. Chudnovsky, Strain-energy effects on dynamic fragmentation, J. Appl. Phys. 59(4) (1986) 1379-1380.

[29] M. Alfreider, D. Kozic, O. Kolednik, D. Kiener, In-situ elastic-plastic fracture mechanics on the microscale by means of continuous dynamical testing, Mater. Des. 148 (2018) 177-187.

[30] Y. Lu, S.S. Xiang, L.R. Xiao, L.H. Wang, Q.S. Deng, Z. Zhang, X.D. Han, Dislocation "bubble-like-effect" and the ambient temperature super-plastic elongation of body-centred cubic single crystalline molybdenum, Sci. Rep. 6 (2016) 8.

[31] J. Marian, W. Cai, V.V. Bulatov, Dynamic transitions from smooth to rough to twinning in dislocation motion, Nat. Mater. 3(3) (2004) 158-163.

[32] D.E. Grady, Shock-wave strength properties of baron carbide and silicon carbide, J. Phys. IV 4(C8) (1994) 385-391.

[33] P.S. Branicio, R.K. Kalia, A. Nakano, P. Vashishta, Shock-induced structural phase transition, plasticity, and brittle cracks in aluminum nitride ceramic, Phys. Rev. Lett. 96(6) (2006) 4.

[34] R. Huang, P. Li, T. Liu, X-ray microtomography and finite element modelling of compressive failure mechanism in cenosphere epoxy syntactic foams, Compos. Struct. 140 (2016) 157-165.

[35] W.C. Duncanhewitt, G.C. Weatherly, Evaluating the hardness, young modulus and fracture-toughness of some pharmaceutical crystals using microindentation techniques, J. Mater. Sci. Lett. 8(11) (1989) 1350-1352.

[36] R.G. Munro, Material properties of a sintered alpha-SiC, J. Phys. Chem. Ref. Data 26(5) (1997) 1195-1203.

List of Tables

Parameter	Value	Reference value [35, 36]
Density (kg m^{-3}), ρ	3075	3160
Young's modulus (GPa), E	385	415
Tensile strength (MPa), σ_{max}	250	250±15
Fracture toughness (MPa $m^{1/2}$), K_{IC}	3.5	3.2±0.6
Reference strain rate (s^{-1}), $\dot{\varepsilon}_0$	1000	-
Damage evolution parameter, k	0.5	-

List of Figures

by the simple closed curves. The FFT patterns in the boxes i and ii are illustrated in the right inset figures.

Fig. 6 Statistic size distribution of the fragments of a silicon carbide specimen under dynamic compression, and the fitted log-normal distribution.

Fig. 7 Prediction of fragment size as a function of strain rates with or without consideration of damage evolution effect.

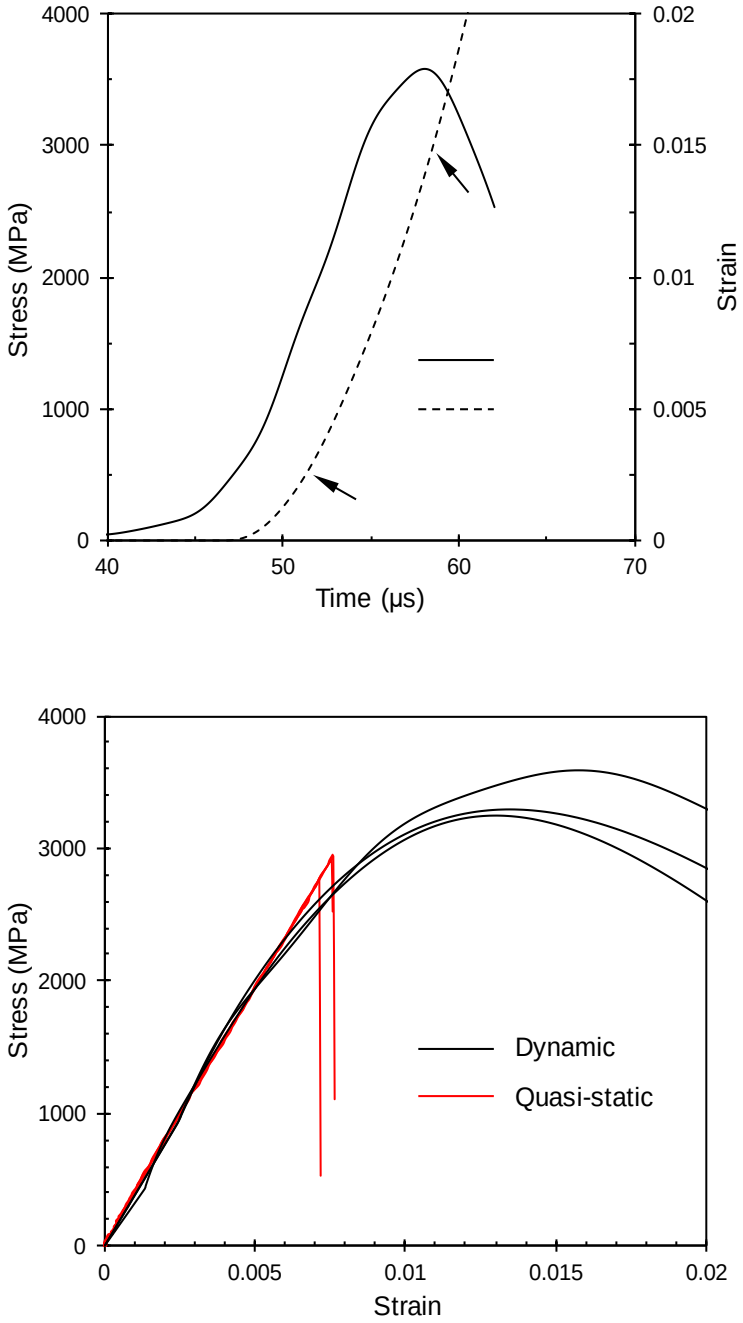

Fig. 1 (a) The stress and strain histories in a silicon carbide specimen as calculated from the strain waves measured in the split-Hopkinson pressure bar test, and (b) representative stress–strain curves at quasi-static and dynamic loading rates.

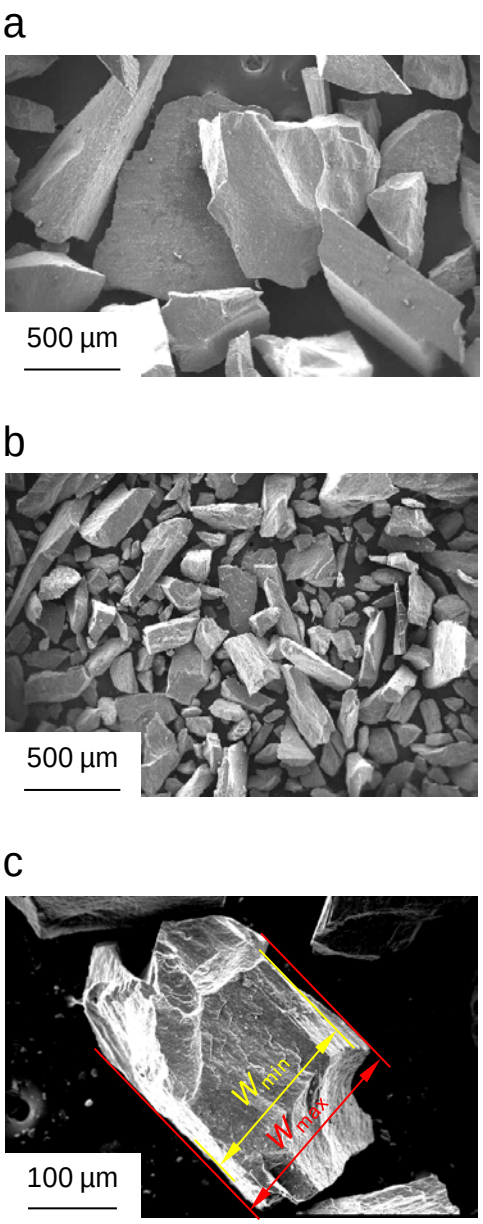

Fig. 2 SEM images of the fragments of silicon carbide specimens subjected to uniaxial compression at (a) quasi-static and (b) dynamic loading rates. Figure (c) shows a typical fragment from the dynamic compression test with the key dimensions marked.

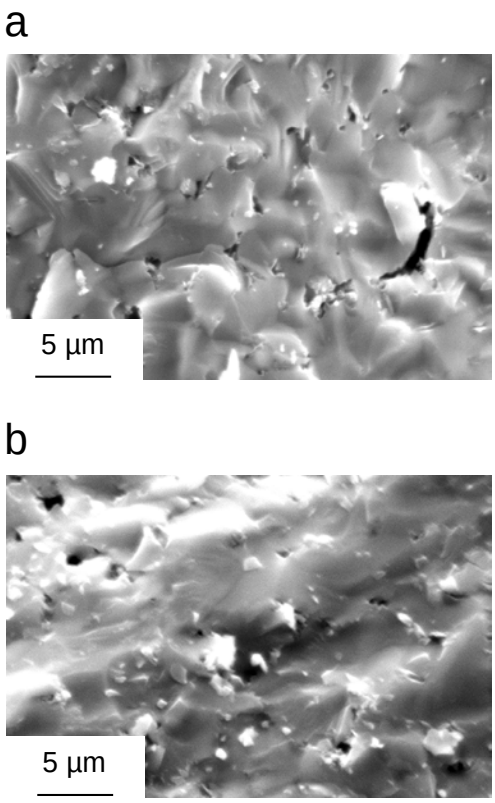

Fig. 3 SEM images of the fracture surface in silicon carbide subjected to (a) quasi-static and (b) dynamic compression.

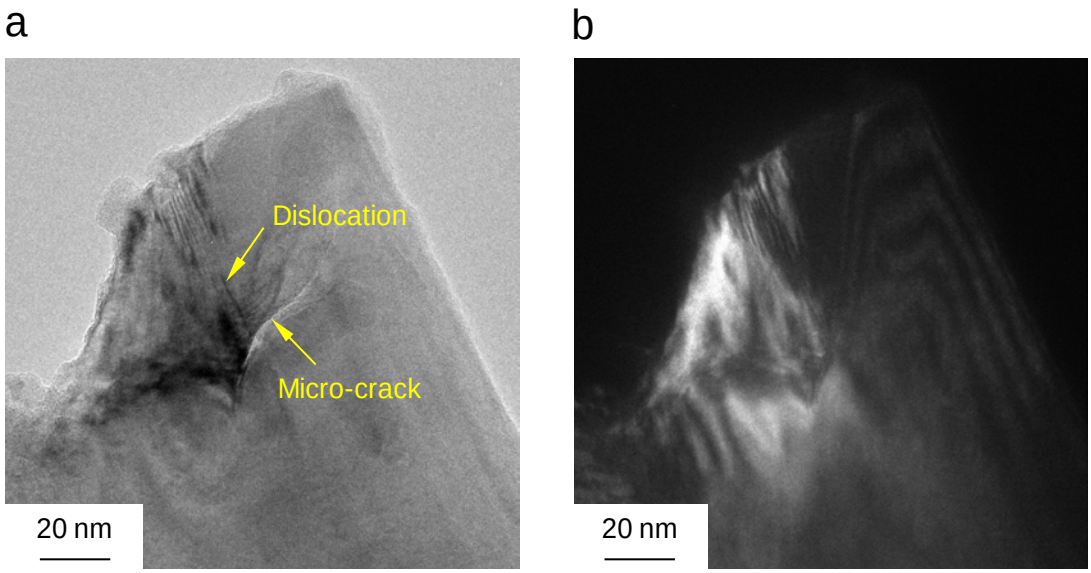

Fig. 4 (a) Bright field and (b) corresponding dark field TEM images of the thin fracture edge in a silicon carbide fragment collected in the dynamic compression test.

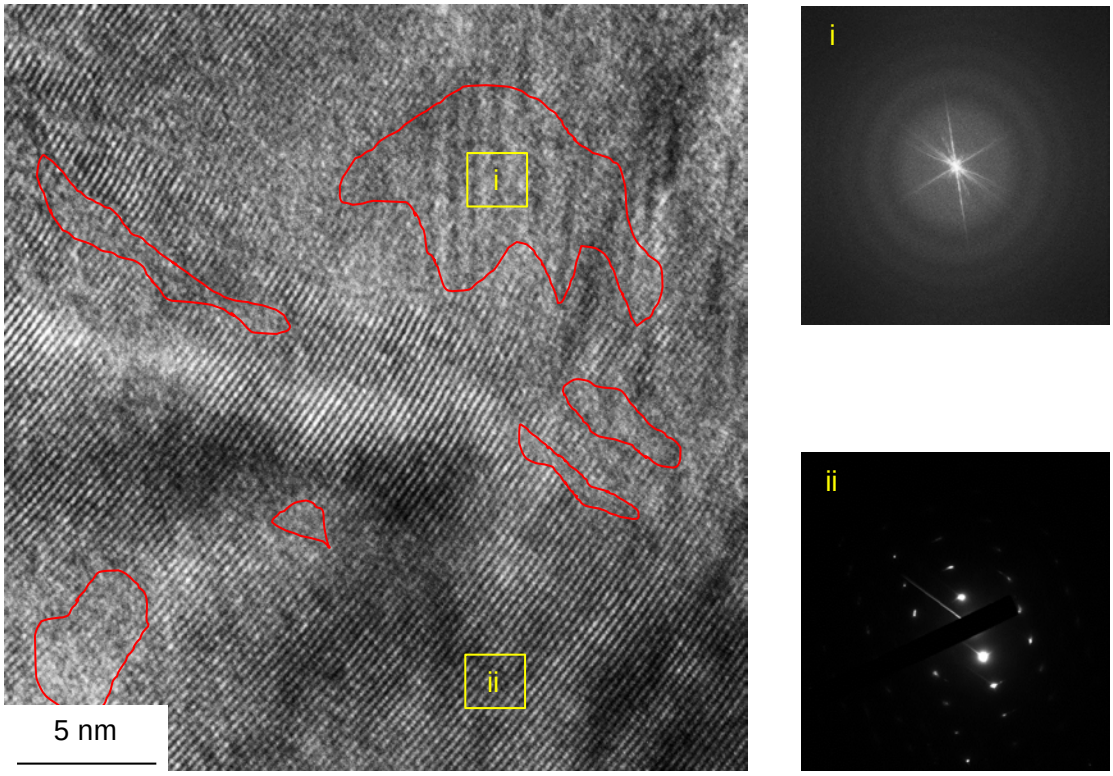

Fig. 5 High resolution TEM lattice image of the crystalline structures and the localised amorphous phases (i.e., loss of crystalline features) as indicated by the simple closed curves. The FFT patterns in the boxes i and ii are illustrated in the right inset figures.

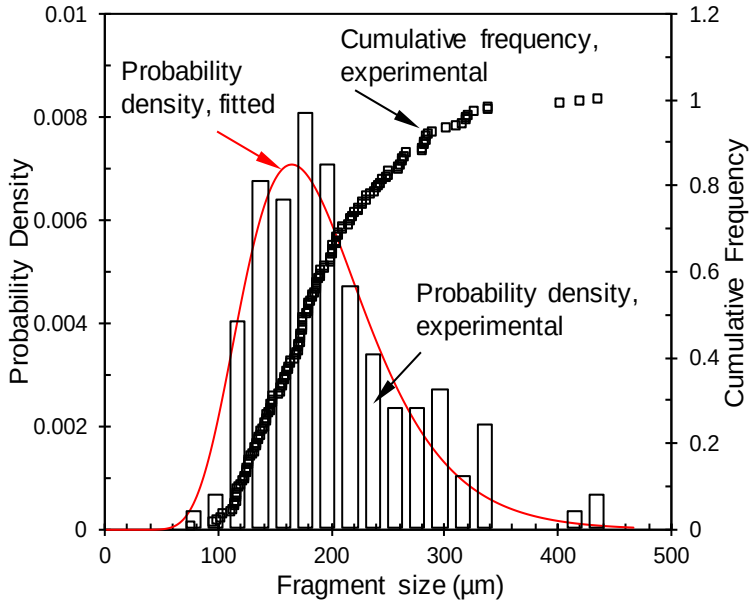

Fig. 6 Statistic size distribution of the fragments of a silicon carbide specimen under dynamic compression, and the fitted log-normal distribution.

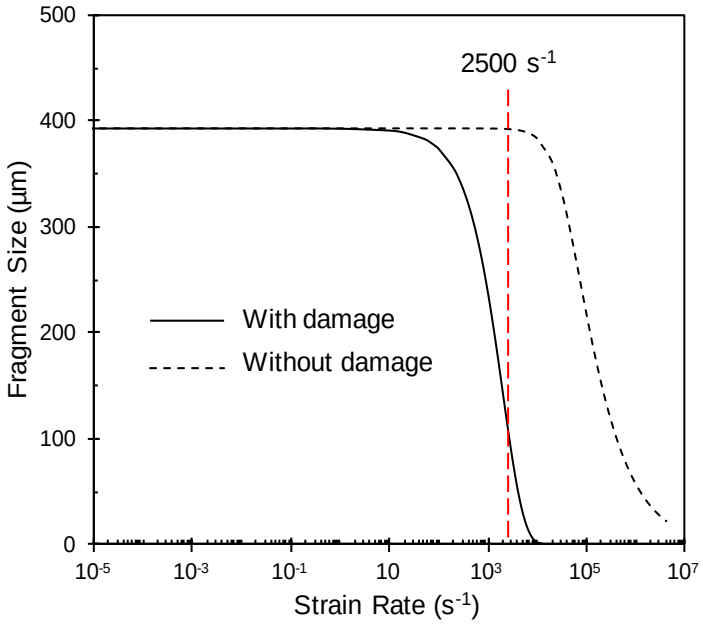

Fig. 7 Prediction of fragment size as a function of strain rates with or without consideration of damage evolution effect.